Sub-micrometer plasma-enhanced chemical vapor deposition using an atmospheric pressure plasma jet localized by a nanopipette scanning probe microscope

OPEN ACCESS
IOP Publishing
Journal of Micromechanics and Microengineering
J. Micromech. Microeng. **32** (2022) 015006 (10pp)
https://doi.org/10.1088/1361-6439/ac3afe

Sub-micrometer plasma-enhanced chemical vapor deposition using an atmospheric pressure plasma jet localized by a nanopipette scanning probe microscope

Sho Yamamoto[1], Kenta Nakazawa[1], Akihisa Ogino[1] and Futoshi Iwata[1,2,3,*]

[1] Graduate School of Integrated Science and Technology, Shizuoka University, JohokuNaka-ku, Hamamatsu, 432-8561, Japan
[2] Graduate School of Medical Photonics, Shizuoka University, JohokuNaka-ku, Hamamatsu, 432-8011, Japan
[3] Research Institute of Electronics, Shizuoka University, JohokuNaka-ku, Hamamatsu, 432-8011, Japan

E-mail: iwata.futoshi@shizuoka.ac.jp

Received 3 September 2021, revised 23 October 2021
Accepted for publication 18 November 2021
Published 6 December 2021

Abstract

We developed a localized plasma-enhanced chemical vapor deposition (PE-CVD) technique to deposit silicon oxide with a sub-micrometer width on a substrate using an atmospheric pressure plasma jet (APPJ) irradiated from a nanopipette nozzle. To realize fine material deposition, hexamethyldisiloxane (HMDSO) vapor was blown into the localized helium APPJ irradiated from the sub-micrometer aperture of the nanpopipette with the jet length limited to the aperture size of the nanopipette. The irradiation distance was controlled using a shear-force positioning technique using scanning probe microscopy (SPM). The proposed system successfully deposited silicon oxide dots with sub-micrometer width on a substrate. After the deposition, the topography of the deposited surface was observed by scanning the nanopipette, which can be used as an SPM probe. The localized PE-CVD properties were systematically investigated by varying the deposition parameters. The amount of deposited material could be controlled by the flow rate of the carrier gas of the HMDSO vapor, APPJ irradiation time, and nanopipette–substrate surface irradiation distance.

Keywords: atmospheric pressure plasma jets, scanning probe microscope, material deposition, plasma enhanced chemical vaper deposition, nanopipette

(Some figures may appear in colour only in the online journal)

* Author to whom any correspondence should be addressed.

1. Introduction

Atmospheric pressure plasmas (APPs) have attracted significant attention as plasmas that can be generated in the atmosphere; thus, their applications are expected to be used in various fields, such as physics [1–7], medicine [8–11], biology [12–17], and engineering [18–27]. In particular, an APP jet (APPJ), which is a jet-like plasma injected from the tip aperture of a tube nozzle under atmospheric pressure [28, 29], has recently been applied to surface material processing and modification. As APPJ does not require a vacuum environment, a simple and inexpensive device configuration can be realized. In general, APPJ is generated in a dielectric tube and irradiated as a plasma bullet through a tube aperture [29]. Therefore, the irradiation area can be localized at a high density, which is useful for maskless fabrication processes. Plasma etching techniques using APPJ have been developed for material removal processing [30–33]. By irradiating the silicon surface with APPJ doped with the etching gas of SF_6, localized dot etching with sub-millimeter widths was achieved. A nozzle with a smaller aperture should be used to realize finer processing using a smaller APPJ. In a previous study, specially designed microcantilevers for localized plasma generated at a pyramidal tip nozzle were proposed [34, 35]. These microcantilevers require complex microfabrication processes and are difficult to use owing to their high manufacturing costs. Previous studies have developed localized APPJs using a nanopipette that can be easily and inexpensively prepared by thermally pulling a capillary glass tube [36–39]. A nanopipette with a tip aperture of sub-micrometer diameter was used not only as a nozzle to generate localized APPJs but also as a probe for scanning probe microscopy (SPM). This allows us to move the tip of the nanopipette close to a material surface with nanometer-scale accuracy using the positioning technique of the SPM and subsequently irradiate the localized APPJ on the material surface. Using this system, we etched sub-micrometer-wide dots and lines on the surface of the photoresist [38] and polymethylmethacrylate [39, 40].

APPJ can be used not only for material removal processing, but also for material deposition techniques, called plasma-enhanced chemical vapor deposition (PE-CVD). PE-CVD techniques have been reported for silicon oxide (SiO_x) and tungsten oxide [41–44]. However, the processing width of PE-CVD is still in the sub-millimeter order. Therefore, to apply APPJ as a microdeposition process for the fabrication of microdevices, such as microelectromechanical systems (MEMS), the processing width should be further reduced.

In this study, we developed a sub-micrometer-sized PE-CVD using the nanopipette positioning technique based on SPM to improve the localization of the material deposition process using APPJ. Hexamethyldisiloxane (HMDSO) was used as the precursor gas. SiO_x, which is used in various applications owing to its excellent properties, such as electrical insulation, wear resistance, hardness, optical transparency, and chemical inertness [45–47], was deposited on the substrate by reacting it with the oxygen radicals generated by the APPJ, which break the chemical bonds of HMDSO. The amount of deposited SiO_x dots was investigated by systematically varying the processing parameters, such as the amount of added HMDSO, plasma irradiation time, and irradiation distance, using the localized PE-CVD system based on the nanopipette SPM.

2. Experimental methods

2.1. Generation of the localized APPJ for PE-CVD of silicon oxide

Figure 1 shows a schematic of the localized APPJ generated using a nanopipette. The nanopipette was fabricated using a capillary borosilicate glass tube (G-1, Narishige, Tokyo, Japan) with an inner and outer tube diameter of 0.6 and 1.0 mm, respectively. The capillary tube was thermally pulled using a commercial laser puller (P-2000, Sutter Instrument Company, USA). The APPJ used in this study was generated using dielectric barrier discharge. The source gas was first introduced into the nanopipette. A tungsten wire inserted in the nanopipette was connected to a high-voltage power supply. When a high-voltage pulse wave was applied to the inner electrode, the He source gas was ionized as the plasma was jetted out from the aperture of the nanopipette tip. As shown in figure 1, the HMDSO vapor (Tokyo Chemical Industry, Tokyo, Japan) with O_2 carrier gas was blown into the APPJ irradiated from the tip of the nanopipette through a nozzle. The CH_3 bonds in HMDSO were broken by APPJ, and oxygen radicals were generated. As a result, a SiO_x film was locally deposited on the substrate via a chemical reaction with oxygen radicals.

2.2. Scanning nanopipette probe microscope for local deposition and observation

Figure 2 shows the experimental setup of the local deposition system using an APPJ based on SPM with a nanopipette. The system consists of a nanopipette positioning system with nanometer-scale accuracy relative to the substrate and a material deposition system using the APPJ ejected from the nanopipette aperture.

Shear force feedback control, a probe positioning technique of SPM, was employed to position the nanopipette in the vicinity of the substrate surface. Shear force is an interactive force between the horizontally oscillating probe tip and the sample surface, which is caused by van der Waals forces and viscous resistance due to the meniscus in the atmosphere [48]. When the nanopipette tip approached the substrate surface while oscillating the tip horizontally at its resonance frequency, the resonance frequency shifted because of the shear force acting between the tip and surface. By detecting a slight frequency shift and maintaining it at a preset constant value through the feedback system, the distance between the pipette tip and substrate surface can be maintained at a constant nanometer level. In the experimental system, the tip of the nanopipette oscillated at the resonance frequency using a piezoelectric (PZT) oscillator. The oscillated tip was projected with a focused beam from a laser diode (LDV167S,

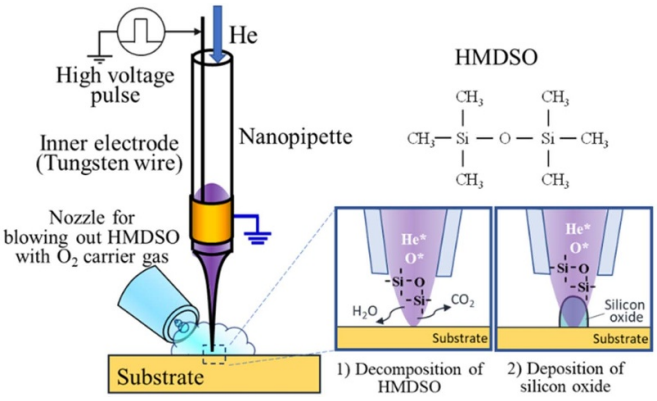

Figure 1. Schematic of the fine PE-CVD using APPJ localized with a nanopipette. The chemical structure of HMDSO decomposed under the irradiation of APPJ and SiO_x is deposited on the substrate.

Takenaka Optronic Co., Ltd, Kyoto, Japan), and the tip oscillation was detected using a photodiode (S4602, Hamamatsu Photonics, Hamamatsu, Japan). The oscillation signal from the photodiode was sequentially detected using an *I–V* converter, an arithmetic circuit, and a self-oscillation circuit. The shift in the resonance frequency due to the shear force was detected by a phase-locked loop (PLL) circuit (OC4, Nanonis/SPECS, Zurich, Switzerland). The output signal of the PLL circuit, corresponding to the frequency shift, was fed to a feedback controller (SC4, Nanonis/SPECS, Zurich, Switzerland) connected to a personal computer. The feedback control system maintained a predefined value of the frequency shift by driving a PZT tube scanner through a PZT driver (HVA4, Nanonis/SPECS, Zurich, Switzerland) to maintain a constant distance between the pipette tip and the material surface with nanometer-scale accuracy. During the material deposition process, the pipette tip was raised to a set distance (irradiation distance) from the position where the pipette tip detected the substrate surface using a pipette edge positioning technique. Subsequently, the deposition process was performed at a constant pipette-tip height. Immediately after the deposition process, the nanopipette was placed close to the surface for detection, and sequential topographic imaging of the deposited structures was performed after deposition under feedback control.

For the local deposition function using APPJ, the flow rate of He gas introduced into the nanopipette was controlled by a mass flow controller (Model 8500MC, Kofloc, Kyoto, Japan). To prevent damage to the nanopipette tip by the localized pressure, a leak orifice with a diameter of 1 mm was fabricated and installed before the inflow of the nanopipette. The pulse wave output from the function generator was amplified to a voltage of several kilovolts using a high-voltage amplifier (HVA4321, NF Electronic Instruments, Tokyo, Japan). By applying the amplified pulse voltage between the inner electrode of the nanopipette and the ground electrode wound outside the nanopipette, APPJ was generated by the dielectric barrier discharged between the electrodes.

To carry the HMDSO vapor, the O_2 carrier gas was also controlled by another mass flow controller (KOFLOC 8500MC) and was subsequently injected into the HMDSO container to introduce the HMDSO vapor to the APPJ using the nozzle. HMDSO temperature was maintained at 25 °C. The deposited SiO_x is chemically stable and physically adsorbed on the substrate; therefore, the dependence on the substrate material is considered to be low. Therefore, in this study, only the slide glass was used as the substrate material, except for the EDX analysis.

3. Results

3.1. EDS analysis of the deposition film

The surface morphology and elemental composition of the deposited film were investigated using a computer-controlled digital scanning electron microscope (SM-7001 F, JEOL, Tokyo, Japan) attached to an energy dispersive x-ray spectrometer (EDS). Here, a nanopipette with an aperture diameter of 100 μm was used for easy analysis, and a gallium arsenide (GaAs) wafer, instead of glass, was used as the substrate to prevent component overlap with the deposit composition. The flow rates of the He source gas and O_2 carrier gas were 400 and 5 sccm, respectively. For the APPJ discharge, the amplitude of the applied pulse voltage was 4 kV_{p-p}, the frequency was 7 kHz, and the pulse duty ratio was 50%. The APPJ irradiation time was set to 20 s.

Figure 3 shows the electron microscopy, EDS spectra, and composition mapping images of the deposited film. The results confirmed the formation of the deposited film in the APPJ irradiation region. The EDS spectra and compositional mapping indicate that the deposit is composed of Si and O, and a small amount of C. Therefore, HMDSO was decomposed by the APPJ, and a fine SiO_x film was formed through localized PE-CVD.

3.2. Sub-micrometer scale deposition of SiO_x using the nanopipette SPM

The sub-micrometer-scale PE-CVD technique was performed using SPM with a nanopipette probe. For the sub-micrometer-scale deposition, a nanopipette with an aperture diameter of 400 nm was employed, and slide glass was used as the substrate. The flow rates of the He source gas and O_2 carrier gas were 400 and 10 sccm, respectively. HMDSO temperature was maintained at 25 °C. For the APPJ discharge, the applied voltage was 3.5 kV_{p-p}, the frequency was 7 kHz, and the pulse duty ratio was 50%. The distance between the pipette tip and substrate surface was 600 nm. The APPJ irradiation time was set to 1 s. Figures 4(a)–(c) show the 2D and 3D images of the topography and line profile of the dots deposited on the substrate, respectively. Four dots with half-bandwidths of approximately 300 nm were deposited on the substrate surface. These results indicate that the local deposition by He-APPJ with HMDSO vapor could be realized with sub-micrometer-scale fabrication. As shown in figure 4, the nanopipette can be used as a nozzle for the APPJ and probe for SPM. Thus, *in situ* observations and evaluations were performed immediately after the deposition process.

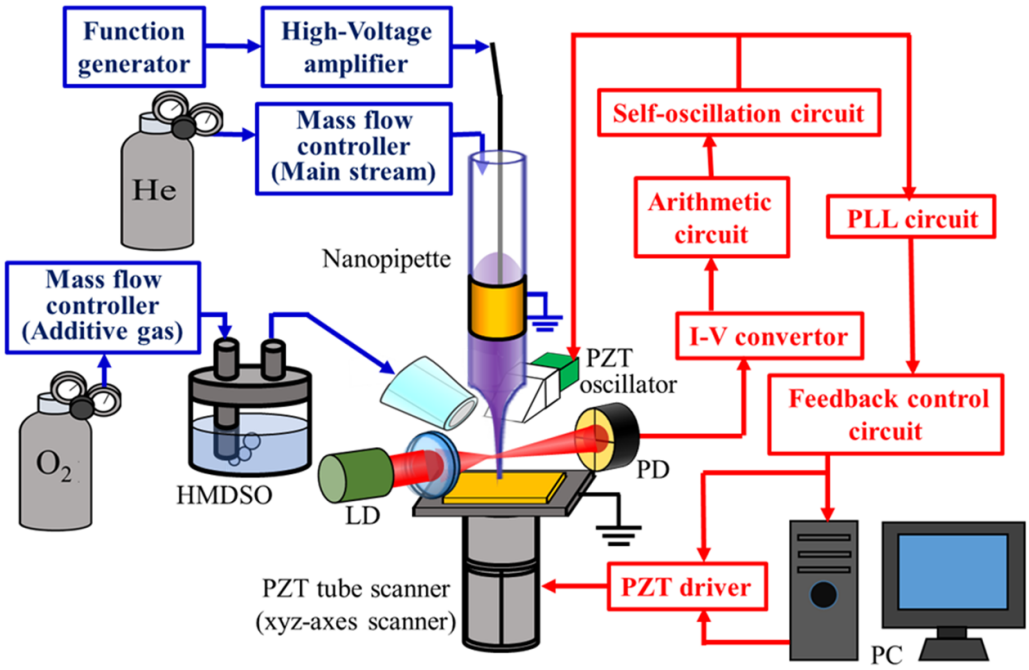

Figure 2. Schematic of the experimental setup of the localized PE-CVD system coupled with the nanopipette SPM.

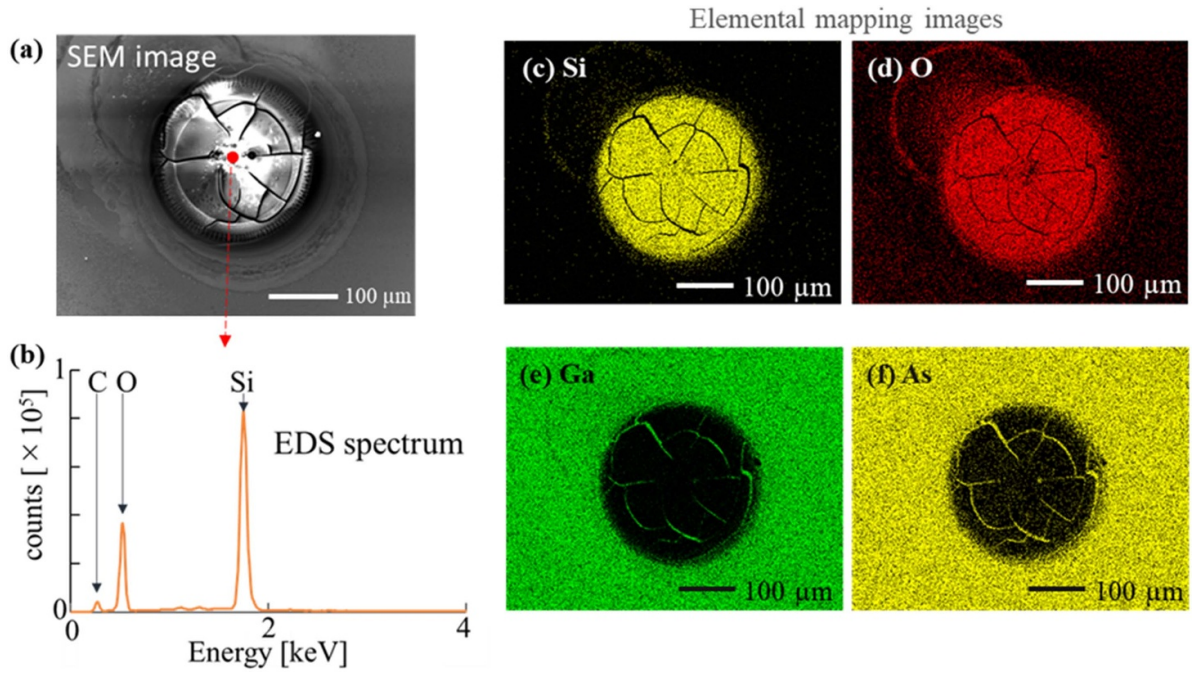

Figure 3. EDS analysis of the locally deposited film formed on GaAs substrate. (a) Electron microscopy image. (b) EDS spectra of the deposited dot. (c)–(f) Compositional mapping images of Si, O, Ga, and As, respectively.

3.3. Dependence of the deposition height on the HMDSO flow rate

As SiO_x deposits are formed by the decomposition of HMDSO, the flow rate of the O_2 carrier gas in the HMDSO vapor was increased from 2 to 10 sccm in 2 sccm increments to evaluate the dependence of the deposit height on the amount of added HMDSO. The flow rate of the He source gas was 400 sccm. For the discharge of the APPJ, the amplitude of the applied pulse voltage was 3.5 kV_{p-p} and the frequency was 7 kHz with a pulse duty ratio of 50%. The APPJ irradiation time was set to 15 s. The distance between the pipette tip and the substrate surface was 600 nm. Figure 5 shows the SPM images and line profiles of the deposited dots when the flow rates of the carrier gas were 0, 4, 6, and 10 sccm. As shown in figure 5(a), there were no deposits formed within the white circles, which represent the irradiation area of the APPJ with a carrier gas flow rate of 0 sccm.

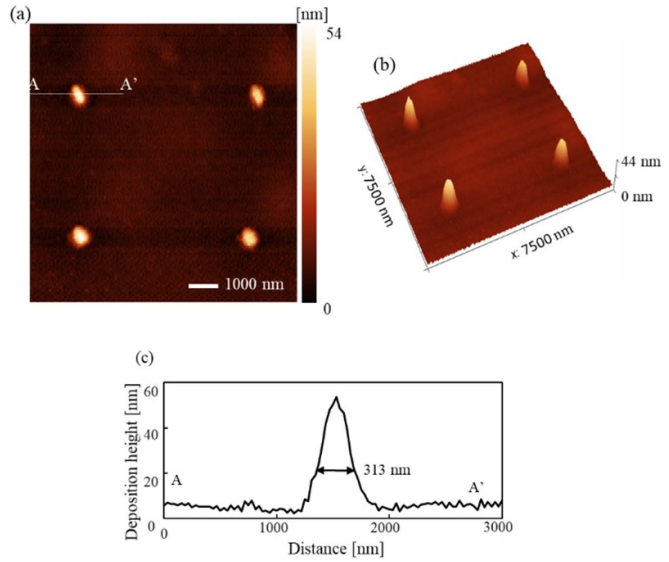

Figure 4. Sub-micrometer scale deposition of four dots on the substrate: (a) 2D topographical image, (b) 3D topographical image, and (c) line profile of the deposited dot.

In contrast, by increasing the carrier gas of the HMDSO vapor, deposits at the sub-micrometer scale were formed in the APPJ-irradiated area, as shown in figures 5(b)–(d).

Figures 5(e) and (f) show the height and width of the deposit depending on the flow rate of the carrier gas, respectively. The width of the dots is shown as the full width at half maximum (FWHM). The error bars indicate the maximum and minimum values, and the plots show the mean values ($n = 3$). The height and width of the deposits increased with an increase in the carrier gas flow rate. This trend can be attributed to the increase in the amount of HMDSO added to the APPJ with an increase in the carrier gas flow rate. Therefore, the amount of deposits can be controlled by controlling the carrier gas flow rate.

In this system, the amount of HMDSO injected into the APPJ was increased by increasing the O_2 used as a carrier gas. However, as O_2 also contributes to the reaction of PE-CVD, it is preferable to evaluate the flow rate by controlling it independently. By using He gas as a carrier gas for HMDSO and then adding O_2 separately, it would be possible to control the flow rate of each gas independently. This will be a topic for future research.

3.4. Dependence of the deposition rate on the irradiation time

The dependence of the deposition rate on the irradiation time was investigated by varying the APPJ irradiation time from 1 to 8 s. The flow rates of the He source gas and O_2 carrier gas were 400 and 10 sccm, respectively. For the APPJ discharge, the amplitude of the applied voltage was 3.8 kV_{p-p}, the frequency was 7 kHz, and the pulse duty ratio was 50%. The distance between the pipette tip and substrate surface was 600 nm. Figures 6(a)–(d) show the SPM images and line profiles at irradiation times of 1, 3, 6, and 8 s, respectively. Figures 6(e) and (f) show the dependence of the deposit height and width on the APPJ irradiation time, respectively. The error bars show the maximum and minimum values, and the plots depict the mean values ($n = 3$). The height and width of the deposit increased with increasing irradiation time. This indicates that the amount of deposits can be controlled by varying the irradiation time. However, the rate of increase in the deposition height gradually decreased with a further increase in the irradiation time.

At irradiation times of less than 3 s, the growth rate of the deposition height was approximately 100 nm s^{-1}. In contrast, the growth rate of the deposition height was less than 30 nm s^{-1} for irradiation times longer than 3 s. In this deposition method, HMDSO vapor was added to the APPJ from outside the nanopipette. Hence, the concentration distribution of the HMDSO vapor might be lower in the immediate vicinity of the pipette tip aperture because of the strong flow of the He source gas ejected from the pipette aperture. In addition, at irradiation times of less than 3 s, the top of the deposit is located far from the aperture of the nanopipette and the HMDSO vapor was sufficiently mixed in this region for efficient deposition. However, at an irradiation time of approximately 3 s, the height of the deposit reached approximately 400 nm, and at longer irradiation times, it tended to saturate. As mentioned above, HMDSO was not sufficiently mixed near the pipette aperture; thus, the efficiency of HMDSO deposition significantly decreased after irradiation for more than 3 s. Even after increasing the irradiation time, the deposition height remained saturated at a position of approximately 100–200 nm below the pipette tip. As discussed in sections 3.2, 3.3, and 3.5, the irradiation time was set to 15 s to ensure that the deposition height settled at the saturated value with less dispersion.

3.5. Dependence of the deposition height on the distance between pipette tip and sample

As the APPJ length emitted from the small aperture of the nanopipette was short, we evaluated the changes in the deposition height when the distance between the nanopipette and substrate surface was varied. The distance between the nanopipette and substrate, that is, the plasma irradiation distance, was varied from 200 to 1400 nm with 200 nm increments. The flow rates of the He source gas and O_2 carrier gas were 400 and 10 sccm, respectively. For the APPJ discharge, the amplitude of the applied pulse voltage was 3.8 kV_{p-p}, the frequency was 7 kHz, and the pulse duty ratio was 50%. The APPJ irradiation time was 15 s.

Figures 7(a)–(d) show the SPM images and line profiles of the deposits at irradiation distances of 200, 600, 1000, and 1400 nm, respectively. Figures 7(e) and (f) show the dependence of the deposition height and width on the nanopipette tip–sample distance, respectively. The error bars show the maximum and minimum values, and the plots indicate the mean values ($n = 3$). The height of the deposit increased with an increase in the irradiation distance. However, at an irradiation distance greater than 1000 nm, the height of the deposit decreased, and the deposition width expanded as the irradiation distance increased. In our previous paper, the irradiation length of the APPJ from the aperture of the nanopipette was approximately 1000 nm [38]. When the irradiation distance

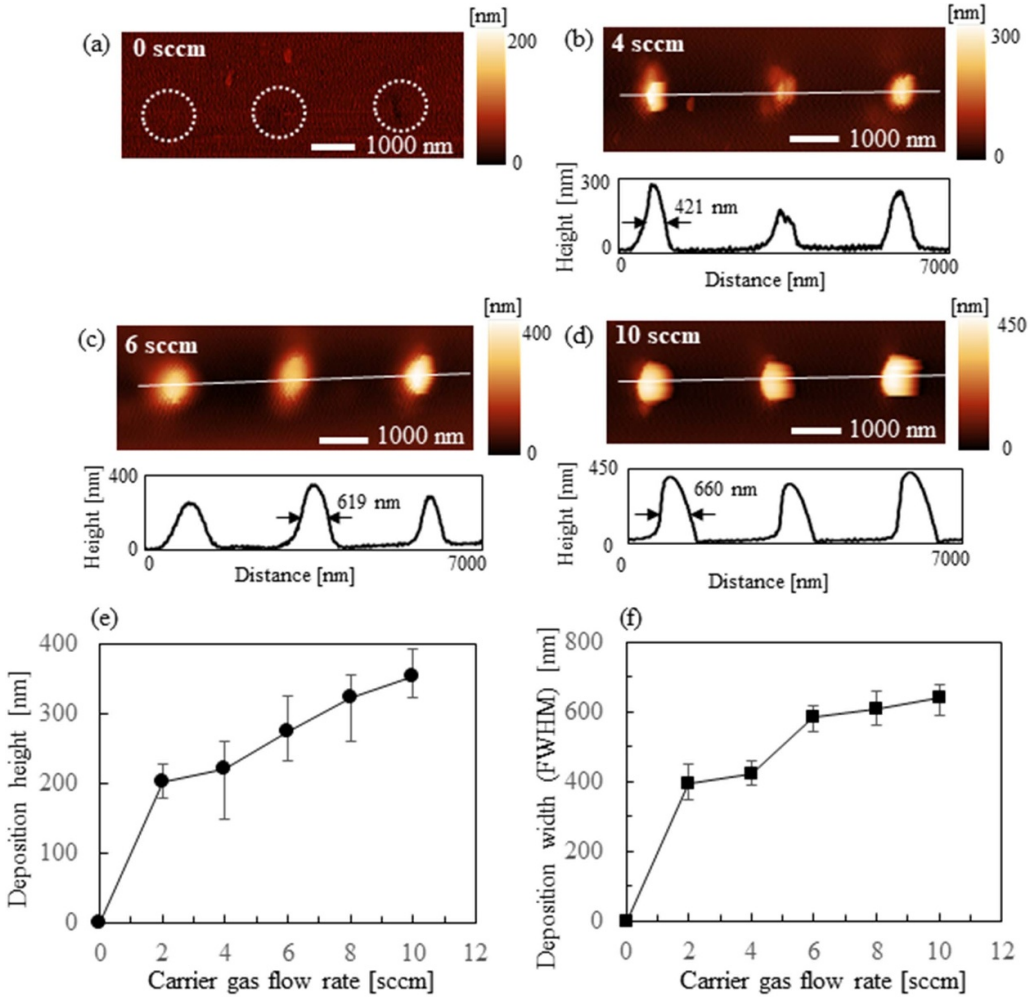

Figure 5. Dependence of the deposition height on the O_2 carrier gas flow rate of the HMDSO vapor. (a)–(d) SPM images and line profiles of the deposited dots when the flow rate of the O_2 carrier gas was 0, 4, 6, and 10 sccm, respectively. (e) Deposition height of the dots as a function of the carrier gas flow rate. (f) Deposition width (FWHM) of the dots as a function of the carrier gas flow rate.

is less than 1000 nm, the plasma jet reaches the substrate, which is produced by the decomposition of HMDSO in the plasma, is deposited on the substrate surface, and the deposits grow close to the nanopipette aperture. However, when the irradiation distance was more than 1000 nm, the plasma jet could not reach the substrate. As a result, the decomposition products are blown away and widely scattered by the gas flow, and subsequently deposited, resulting in a significant decrease in the deposition efficiency. Therefore, to control the amount of material deposited on the substrate, the plasma irradiation distance should be precisely controlled using the SPM system.

4. Discussion

As described above, the amount of SiO_x deposition depends on several parameters, such as the flow rate of the carrier gas of the HMDSO vapor, irradiation time of the APPJ, and irradiation distance from the nanopipette, indicating that the material deposition rate can be controlled by varying these parameters.

The irradiation distance that can be deposited can be slightly extended by increasing the He flow rate of the plasma source gas. However, on increasing the He flow rate, the gas did not mix with the HMDSO gas near the pipette aperture because of the strong gas flow, resulting in a decrease in the processing accuracy of the deposited film. In addition, when the flow rate was excessively low, the plasma became unstable. Therefore, to ensure stable plasma and relatively accurate deposition near the pipette tip, a He flow rate of 400 sccm was set as the optimal flow rate in this experiment.

As for the deposition rate compared with existing methods, the deposition rate of the SiO_x films by PE-CVD using general low-pressure plasma is several tens of nm/min, with a power consumption of several tens to several hundred watts [49, 50]. In the case of the APP, the deposition rate is several tens of nm/s, with a power consumption of several hundred watts [51–53]. By contrast, in the proposed method, as shown in figure 7, the deposition height reached 700 nm when the irradiation distance was 1000 nm, which corresponds to an average deposition rate of 46 nm s^{-1} for an irradiation time of 15 s. The power consumption of the local irradiation of APPJ

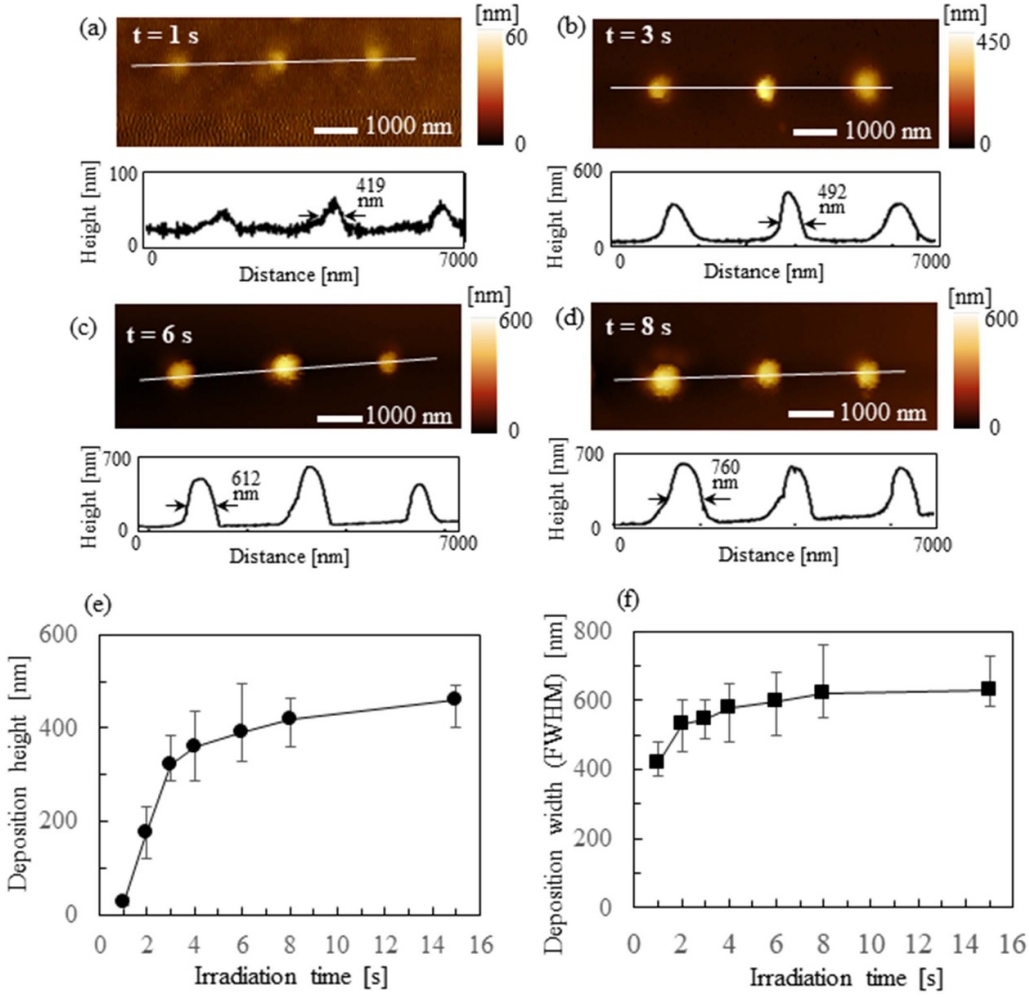

Figure 6. Dependence of the deposition height on the irradiation time. (a)–(d) SPM images and line profiles at the irradiation times of 1, 3, 6, and 8 s, respectively. (e) Deposition height of the dots as a function of the APPJ irradiation time. (f) Deposition width (FWHM) of the dots as a function of the APPJ irradiation time.

using the nanopipette in this system was estimated to be 0.8 W based on the measured current and voltage; this is consistent with the reported power consumption of less than 1 W for similar APPJ irradiation systems using nanopipettes [54]. Thus, the proposed method can achieve a high deposition rate with low power consumption.

With regard to the processing accuracy of the deposition using this method, the error bars shown for the deposition heights in figures 5(e)–7(e) show that the difference between the average value and the maximum or minimum value is approximately 10%. However, some of the differences were as large as 30%. This may be due to the variability in the plasma intensity. It is difficult to adjust the flow rate of the He source gas introduced into the nanopipette, and the amount of irradiation from the pipette tip aperture is likely to vary slightly, resulting in variations in the plasma intensity. It has also been reported that the O_2 used for the addition of HMDSO destabilizes plasma operation [55]. In addition, factors that cause SiO_x microcrystals to be blown off the substrate (without adhering to it) by the gas flow may also cause variations in the amount of deposition. Therefore, to improve the processing accuracy, it is necessary to optimize various parameters within the range of stabilizing the plasma intensity.

The sub-micrometer-scale PE-CVD technique based on the nanopipette SPM developed in this study can be used to develop fine deposition methods for various materials using other additive gases and is expected to be applied to various fields, such as maskless patterning of microdevices. One of the potential applications of the proposed method is post-fabrication technology to compensate for the process variations in MEMS manufacturing. Process variations, such as the structural material not being deposited uniformly or not being etched accurately, often occur in MEMS manufacturing. As a result, the mechanical and electrical characteristics differ from the design specifications. Therefore, to improve the yield rate and manufacture devices that meet the design specifications, it is necessary to deposit materials locally on a part of the positioned structure as a post-processing modification. For example, tuning the resonant frequency of a MEMS resonator [56–58], which is widely used in sensors, filters, and vibration

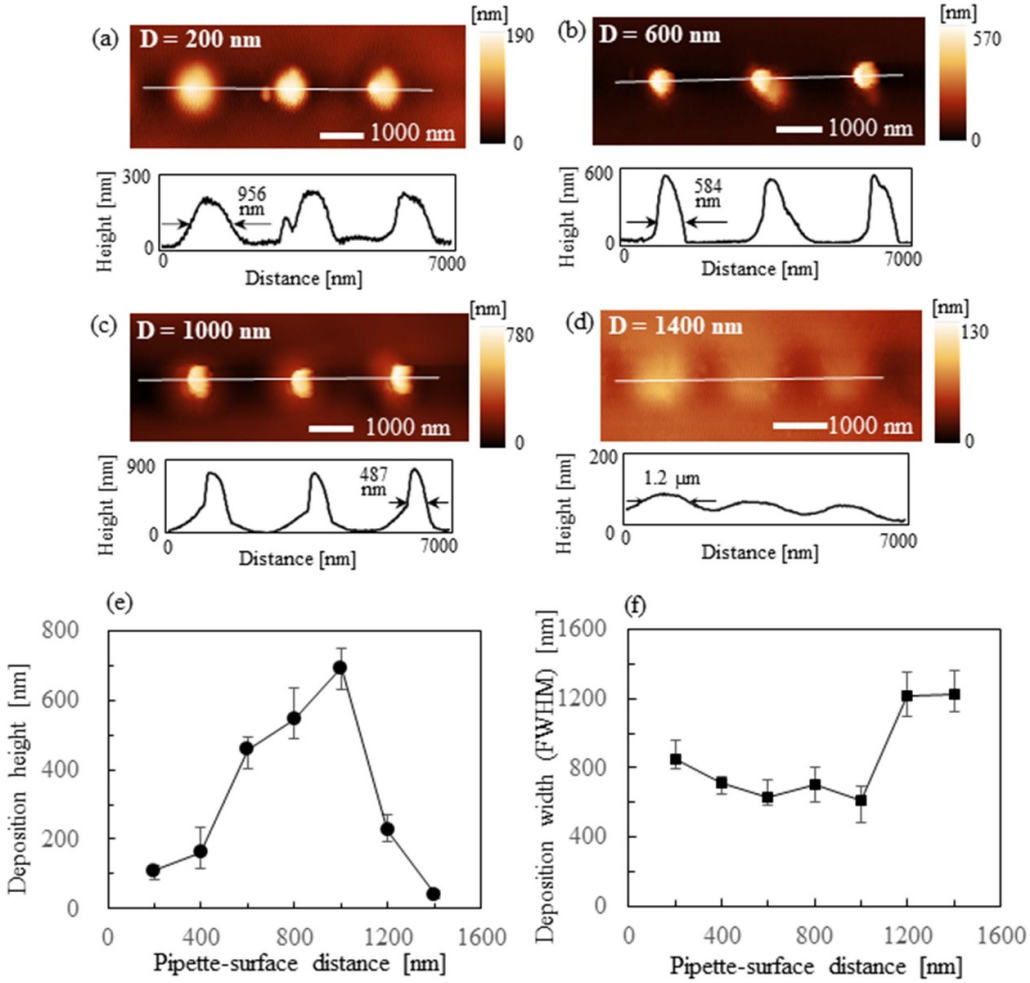

Figure 7. Dependence of the deposition height on the distance between the pipette tip and sample. (a)–(d) SPM images and line profiles at the plasma irradiation distances of 200, 600, 1000, and 1400 nm, respectively. (e) Deposition height of the dots as a function of the pipette–surface distance. (f) Deposition width (FWHM) of the dots as a function of the pipette–surface distance.

power generation, via local deposition on the vibrating body, is an effective application of the proposed technique.

5. Conclusion

We developed a sub-micrometer-scale PE-CVD technique using a nanopipette as a nozzle for APPJ and a probe for SPM. By adding HMDSO vapor to the APPJ irradiated from the nanopipette aperture, HMDSO was decomposed and deposited on the substrate. EDS analysis and compositional mapping of the locally deposited film showed that the deposited film was mainly composed of Si and O, confirming the decomposition of the HMDSO vapors by the APPJ and their deposition as SiO_x. The deposition process using the nanopipette with a sub-micrometer aperture demonstrated reproducible material deposition with a sub-micrometer width using the proposed method. The deposit height increased with an increase in the flow rate of the O_2 carrier gas of the HMDSO vapor and the irradiation time of the APPJ. When the distance between the pipette and substrate was varied, the deposition height increased with an increase in the irradiation distance up to 1000 nm, where the APPJ emitted from the nanopipette aperture reached the substrate. Therefore, by optimizing these parameters, the proposed method could enable fine patterning with a controllable amount of material deposition.

Data availability statement

All data that support the findings of this study are included within the article (and any supplementary files).

Acknowledgments

This work was supported by JSPS KAKENHI Grant Number JP 17H03156 from the Japan Society for the Promotion of Science (JSPS) and a reserach grant from Suzuki Foundation in Japan. We also thank Professor M Ishikawa for helpful support at the Hamamatsu campus center for instrumental analysis at Shizuoka University.

ORCID iDs

Kenta Nakazawa https://orcid.org/0000-0001-7496-2550
Futoshi Iwata https://orcid.org/0000-0002-2048-7579

References

[1] Norberg S A, Johnsen E and Kushner M J 2015 Helium atmospheric pressure plasma jets touching dielectric and metal surfaces *J. Appl. Phys.* **118** 013301

[2] Basher A H and Mohamed A-A H 2018 Laminar and turbulent flow modes of cold atmospheric pressure argon plasma jet *J. Appl. Phys.* **123** 193302

[3] Jõgi I, Talviste R, Raud S, Raud J, Plank T, Moravský L, Klas M and Matejčík Š 2020 Comparison of two cold atmospheric pressure plasma jet configurations in argon *Contrib. Plasma Phys.* **60** e201900127

[4] Walsh J L, Shi J J and Kong M G 2006 Contrasting characteristics of pulsed and sinusoidal cold atmospheric plasma jets *Appl. Phys. Lett.* **88** 171501

[5] Ogawa K, Yajima H, Oh J-S, Furuta H and Hatta A 2019 Effects of sheath gas flow on He atmospheric pressure plasma jet *Appl. Phys. Express* **12** 036001

[6] Gazeli K, Svarnas P, Vafeas P, Papadopoulos P K, Gkelios A and Clément F 2013 Investigation on streamers propagating into a helium jet in air at atmospheric pressure: electrical and optical emission analysis *J. Appl. Phys.* **114** 103304

[7] Wu S, Liu X, Mao W, Chen W, Liu C and Zhang C 2018 Non-thermal air plasma jets at atmospheric pressure: the flow-dependent propagation in the afterglow *J. Appl. Phys.* **124** 243302

[8] Laroussi M and Lu X 2005 Room-temperature atmospheric pressure plasma plume for biomedical applications *Appl. Phys. Lett.* **87** 113902

[9] Kolb J F, Mohamed A-A H, Price R O, Swanson R J, Bowman A, Chiavarini R L, Stacey M and Schoenbach K H 2008 Cold atmospheric pressure air plasma jet for medical applications *Appl. Phys. Lett.* **92** 241501

[10] Fridman G, Friedman G, Gutsol A, Shekhter A B, Vasilets V N and Fridman A 2008 Applied plasma medicine *Plasma Process. Polym.* **5** 503–33

[11] Hirata T, Kishimoto T, Tsutsui C, Kanai T and Mori A 2013 Healing burns using atmospheric pressure plasma irradiation *Jpn. J. Appl. Phys.* **53** 010302

[12] Kumagai S, Chang C-Y, Jeong J, Kobayashi M, Shimizu T and Sasaki M 2015 Development of plasma-on-chip: plasma treatment for individual cells cultured in media *Jpn. J. Appl. Phys.* **55** 01AF01

[13] Kim J Y, Wei Y, Li J and Kim S-O 2010 15-μm-sized single-cellular-level and cell-manipulatable microplasma jet in cancer therapies *Biosens. Bioelectron.* **26** 555–9

[14] Shaw P, Kumar N, Kwak H S, Park J H, Uhm H S, Bogaerts A, Choi E H and Attri P 2018 Bacterial inactivation by plasma treated water enhanced by reactive nitrogen species *Sci. Rep.* **8** 11268

[15] Utsumi F, Kajiyama H, Nakamura K, Tanaka H, Mizuno M, Ishikawa K, Kondo H, Kano H, Hori M and Kikkawa F 2013 Effect of indirect nonequilibrium atmospheric pressure plasma on anti-proliferative activity against chronic chemo-resistant ovarian cancer cells *in vitro* and *in vivo PLoS One* **8** e81576

[16] Akhavan B *et al* 2018 Plasma activated coatings with dual action against fungi and bacteria *Appl. Mater. Today* **12** 72–84

[17] Tanaka H, Mizuno M, Ishikawa K, Nakamura K, Kajiyama H, Kano H, Kikkawa F and Hori M 2011 Plasma-activated medium selectively kills glioblastoma brain tumor cells by down-regulating a survival signaling molecule, AKT kinase *PMED* **1** 265–77

[18] Noeske M, Degenhardt J, Strudthoff S and Lommatzsch U 2004 Plasma jet treatment of five polymers at atmospheric pressure: surface modifications and the relevance for adhesion *Int. J. Adhes. Adhes.* **24** 171–7

[19] Ichiki R, Inoue T, Yoshimitsu Y, Yamamoto H, Kanda S, Yoshida M, Akamine S and Kanazawa S 2014 Peculiar relationship of plume brightness and hard layer formation in atmospheric-pressure plasma jet nitriding *IEEE Trans. Plasma Sci.* **42** 2466–7

[20] Ito Y, Urabe K, Takano N and Tachibana K 2008 High speed deposition of SiO2 films with plasma jet based on capillary dielectric barrier discharge at atmospheric pressure *Appl. Phys. Express* **1** 067009

[21] Yoshiki H, Ikeda K, Wakaki A, Togashi S, Taniguchi K and Horiike Y 2003 Localized plasma processing of materials using atmospheric-pressure microplasma jets *Jpn. J. Appl. Phys.* **42** 4000

[22] Sung Y-C, Wei T-C, Liu Y-C and Huang C 2018 Silicon etching of difluoromethane atmospheric pressure plasma jet combined with its spectroscopic analysis *Jpn. J. Appl. Phys.* **57** 06JH02

[23] Baniya H B, Guragain R P, Baniya B and Subedi D P 2020 Cold atmospheric pressure plasma jet for the improvement of wettability of polypropylene *Int. J. Polym. Sci.* **2020** e3860259

[24] Kwon O-J, Myung S-W, Lee C-S and Choi H-S 2006 Comparison of the surface characteristics of polypropylene films treated by Ar and mixed gas (Ar/O2) atmospheric pressure plasma *J. Colloid Interface Sci.* **295** 409–16

[25] Rodriguez-Santiago V, Vargas-Gonzalez L, Bujanda A A, Baeza J A, Fleischman M S, Yim J H and Pappas D D 2013 Modification of silicon carbide surfaces by atmospheric pressure plasma for composite applications *ACS Appl. Mater. Interfaces* **5** 4725–30

[26] Mercado-Cabrera A, Jaramillo-Sierra B, López-Callejas R, Valencia-Alvarado R, de La Piedad-beneitez A, Peña-Eguiluz R, Barocio-Delgado S, Muñoz-Castro A and Rodríguez-Méndez B 2013 Surface modification of polypropylene fiber for hydrophilicity enhancement aided by DBD plasma *Prog. Org. Coat.* **76** 1858–62

[27] Cahyani M R, Zuhaela I A, Saraswati T E, Kusumandari A M, Suselo Y H and Ismayenti L 2021 Time dependence of the concentration of dissolved ozone in water generated by dielectric barrier discharge (DBD) plasma using atmospheric air *J. Phys. Conf. Ser.* **1912** 012008

[28] Schutze A, Jeong J Y, Babayan S E, Park J, Selwyn G S and Hicks R F 1998 The atmospheric-pressure plasma jet: a review and comparison to other plasma sources *IEEE Trans. Plasma Sci.* **26** 1685–94

[29] Teschke M, Kedzierski J, Finantu-Dinu E G, Korzec D and Engemann J 2005 High-speed photographs of a dielectric barrier atmospheric pressure plasma jet *IEEE Trans. Plasma Sci.* **33** 310–1

[30] Paetzelt H, Böhm G and Arnold T 2015 Etching of silicon surfaces using atmospheric plasma jets *Plasma Sources Sci. Technol.* **24** 025002

[31] Li Q, Liu J, Dai Y, Xiang W, Zhang M, Wang H and Wen L 2016 Fabrication of SiNx thin film of micro dielectric barrier discharge reactor for maskless nanoscale etching *Micromachines* **7** 232

[32] Senba H, Suzuki H and Toyoda H 2018 Atmospheric pressure water-vapor plasma in an air-shielded environment by water flow *Jpn. J. Appl. Phys.* **58** SAAC05

[33] Ideno T and Ichiki T 2006 Maskless etching of microstructures using a scanning microplasma etcher *Thin Solid Films* **506–507** 235–8

[34] Wen L, Wang H, He L, Zhang Q, Xiang W and Chu J 2011 Design and fabrication of microcantilever probe integrated with microplasma reactor for maskless scanning plasma etching *Sensors Actuators* A **169** 362–6

[35] Xie Y, Yuan W, Tabib-Azar M and Mastrangelo C H 2010 Microfabrication of plasma nanotorch tips for localized etching and deposition *2010 IEEE Sensors* pp 2243–6

[36] Kakei R, Ogino A, Iwata F and Nagatsu M 2010 Production of ultrafine atmospheric pressure plasma jet with nano-capillary *Thin Solid Flms* **518** 3457–60
[37] Motrescu I and Nagatsu M 2016 Nanocapillary atmospheric pressure plasma jet: a tool for ultrafine maskless surface modification at atmospheric pressure *ACS Appl. Mater. Interfaces* **8** 12528–33
[38] Morimatsu D, Sugimoto H, Nakamura A, Ogino A, Nagatsu M and Iwata F 2016 Development of a scanning nanopipette probe microscope for fine processing using atmospheric pressure plasma jet *Jpn. J. Appl. Phys.* **55** 08NB15
[39] Nakazawa K, Yamamoto S, Nakagawa E, Ogino A, Shimomura M and Iwata F 2020 Atmospheric He/O2 plasma jet fine etching with a scanning probe microscope *AIP Adv.* **10** 095103
[40] Toda S, Nakazawa K, Ogino A, Shimomura M and Iwata F 2021 Micromachining of polymers using atmospheric pressure inductively coupled helium plasma localized by a scanning nanopipette probe microscope *J. Micromech. Microeng.* **31** 065008
[41] Janietz M and Arnold T 2011 Surface figuring of glass substrates by local deposition of silicon oxide with atmospheric pressure plasma jet *Surf. Coat. Technol.* **205** S351–4
[42] Kasih T P, Kuroda S and Kubota H 2007 A nonequilibrium, atmospheric-pressure argon plasma torch for deposition of thin silicon dioxide films *Chem. Vapor Depos.* **13** 169–75
[43] Shimizu Y, Bose A C, Mariotti D, Sasaki T, Kirihara K, Suzuki T, Terashima K and Koshizaki N 2006 Reactive evaporation of metal wire and microdeposition of metal oxide using atmospheric pressure reactive microplasma jet *Jpn. J. Appl. Phys.* **45** 8228
[44] Holländer A and Abhinandan L 2003 Localized deposition by μ-jet-CVD *Surf. Coat. Technol.* **174–175** 1175–7
[45] Raballand V, Benedikt J, Hoffmann S, Zimmermann M and Von Keudell A 2009 Deposition of silicon dioxide films using an atmospheric pressure microplasma jet *J. Appl. Phys.* **105** 083304
[46] Takahashi M, Sugimoto K and Maeda R 2005 Nanoimprint of glass materials with glassy carbon molds fabricated by focused-ion-beam etching *Jpn. J. Appl. Phys.* **44** 5600
[47] Zhao Y, Huang C, Huang X, Huang H, Zhao H, Wang S and Liu S 2020 Effectiveness of PECVD deposited nano-silicon oxide protective layer for polylactic acid film: barrier and surface properties *Food Packag. Shelf Life* **25** 100513
[48] Karrai K and Tiemann I 2000 Interfacial shear force microscopy *Phys. Rev.* B **62** 13174–81
[49] Patelli A, Vezzù S, Zottarel L, Menin E, Sada C, Martucci A and Costacurta S 2009 SiO_x-based multilayer barrier coatings produced by a single PECVD process *Plasma Process. Polym.* **6** S665–70
[50] Delimi A, Coffinier Y, Talhi B, Boukherroub R and Szunerits S 2010 Investigation of the corrosion protection of SiO_x-like oxide films deposited by plasma-enhanced chemical vapor deposition onto carbon steel *Electrochim. Acta* **55** 8921–7 Elsevier Enhanced Reader
[51] Schäfer J, Hnilica J, Šperka J, Quade A, Kudrle V, Foest R, Vodák J and Zajčková L 2016 Tetrakis(trimethylsilyloxy)silane for nanostructured SiO2-like films deposited by PECVD at atmospheric pressure *Surf. Coat. Technol.* **295** 112–8
[52] Hnilica J, Schäfer J, Foest R, Zajíčková L and Kudrle V 2013 PECVD of nanostructured SiO_2 in a modulated microwave plasma jet at atmospheric pressure *J. Phys. D: Appl. Phys.* **46** 335202
[53] Li N, Wu Y L, Hong J, Shchelkanov I A and Ruzic D N 2015 SiO_x deposition on polypropylene-coated paper with a dielectric barrier discharge at atmospheric pressure *IEEE Trans. Plasma Sci.* **43** 3205–10
[54] Abuzairi T, Okada M, Bhattacharjee S and Nagatsu M 2016 Surface conductivity dependent dynamic behaviour of an ultrafine atmospheric pressure plasma jet for microscale surface processing *Appl. Surf. Sci.* **390** 489–96
[55] Jeong J Y, Babayan S E, Tu V J, Park J, Henins I, Hicks R F and Selwyn G S 1998 Etching materials with an atmospheric-pressure plasma jet *Plasma Sources Sci. Technol.* **7** 282–5
[56] Joachim D and Lin L 2003 Characterization of selective polysilicon deposition for MEMS resonator tuning *J. Microelectromech. Syst.* **12** 193–200
[57] Chiao M and Lin L 2004 Post-packaging frequency tuning of microresonators by pulsed laser deposition *J. Micromech. Microeng.* **14** 1742–7
[58] Enderling S, Hedley J, Jiang L, Cheung R, Zorman C, Mehregany M and Walton A J 2006 Characterization of frequency tuning using focused ion beam platinum deposition *J. Micromech. Microeng.* **17** 213–9